Quantum transport in the three-dimensional Dirac semimetal Cd$_3$As$_2$

L. P. He, X. C. Hong, J. K. Dong, J. Pan, Z. Zhang, J. Zhang & S. Y. Li[*]

State Key Laboratory of Surface Physics, Department of Physics, and Laboratory of Advanced Materials, Fudan University, Shanghai 200433, China

The material termed three-dimensional (3D) Dirac semimetal has attracted great interests recently, since it is an electronic analogue to two-dimensional graphene[1-8]. Soon after the theoretical predictions of BiO$_2$, A$_3$Bi (A = Na, K, Rb), and Cd$_3$As$_2$ as candidates of 3D Dirac semimetal[1-3], the angle-resolve photoemission spectroscopy experiments indeed observed 3D Dirac points in Na$_3$Bi and Cd$_3$As$_2$ (ref. 4-7). The scanning tunnelling microscopy measurements also support Dirac-like dispersion in Cd$_3$As$_2$ (ref. 8). Here we report quantum transport properties of Cd$_3$As$_2$ single crystal in magnetic field. A sizable linear quantum magnetoresistance is found near room temperature, which indicates the existence of linear gapless energy dispersion. Below 100 K, strong Shubnikov-de Haas oscillations appear in the longitudinal resistivity with a single frequency F = 58.3 T. The linear dependence of Landau index n on $1/B$ gives an n-axis intercept 0.58, which reveals the nontrivial π Berry's phase expected for 3D Dirac fermions. These quantum transport results provide strong bulk evidences for a 3D Dirac semimetal phase in Cd$_3$As$_2$.

The Dirac materials whose excitations obey a relativistic Dirac-like equation have been widely studied in recent years, represented by graphene and topological insulators[8-10]. More recently, a new kind of Dirac material termed 3D Dirac semimetal has been theoretical predicted, with examples of BiO_2, A_3Bi (A = Na, K, Rb), and Cd_3As_2 (ref. 1-3). The 3D Dirac semimetal contains 3D Dirac points with linear energy dispersion in any momentum direction. The 3D Dirac point is protected by crystal symmetry, where two Weyl points overlap in momentum space[1-3]. This kind of fascinating material is a 3D analogue to graphene, which could be important for future device applications.

Following these predictions, the angle-resolved photoemission spectroscopy (ARPES) experiments were carried out on both Na_3Bi and Cd_3As_2 single crystals to probe the unique electronic structure[4-7]. Amazingly, two bulk 3D Dirac points were observed in both compounds, which locate on the opposite sides of the Brillouin zone center point Γ[4-7]. Recent scanning tunnelling microscopy (STM) measurements on Cd_3As_2 single crystal also support the existence of 3D Dirac points[8].

Bulk quantum transport measurement is another important tool to reveal the existence of Dirac fermions. The linear quantum magnetoresistance (*MR*) is a characteristic transport property for Dirac-like energy dispersion, as has previously been observed in β-Ag_2Te, Bi_2Se_3, and Bi_2Te_3 (ref. 12-18). For both Na_3Bi and Cd_3As_2, such a linear quantum *MR* was predicted, even at room temperature[2,3]. Via analysis of the Shubnikov-de Haas (SdH) effect in magnetic field, a nontrivial π Berry's phase is expected for Dirac fermions, which was indeed found in graphene, highly oriented pyrolytic graphite, Bi_2Se_3, Bi_2Te_3, and BiTeI (ref. 17, 19-22). Due to the high sensitivity to air, Na_3Bi is

not suitable for transport measurements. Here we present the longitudinal resistivity and transverse Hall resistance measurements on Cd_3As_2 single crystals in magnetic field. We demonstrate the existence of 3D Dirac semimetal phase in Cd_3As_2 by observing linear quantum *MR* near room temperature and a nontrivial π Berry's phase with phase shift.

Figure 1a shows the temperature dependence of the longitudinal resistivity ρ_{xx} at zero magnetic field for Cd_3As_2 single crystal, which exhibits a metallic-like behaviour. Below 10 K the curve is very flat, giving the residual resistivity $\rho_{xx0} = 28.2$ $\mu\Omega$ cm. Figure 1b presents the Hall resistance R_{xy} as a function of magnetic field from 200 K down to 1.5 K. The negative slope of R_{xy} means that the dominant charge carriers in Cd_3As_2 are electrons, and the carrier concentration $n_e \approx 5.3 \times 10^{18}$ cm^{-3} is estimated from the low-field slope. We evaluate the carrier mobility at 1.5 K by $\mu(1.5K) = 1/n_e\rho_{xx}(1.5K)e \approx 4.1 \times 10^4$ cm^2/Vs, where $\rho_{xx}(1.5K) = 28.2$ $\mu\Omega$ cm and $e = 1.6 \times 10^{-19}$ C. The low concentration and high mobility of charge carriers are well known in Cd_3As_2 (ref. 6-8).

In Fig. 1b, the SdH oscillations of R_{xy} are already visible blow 50 K. The ρ_{xx} shows even pronounced oscillations, as can be seen from the longitudinal *MR* in Fig. 1c. The *MR* is defined by $MR = (\rho_{xx}(B) - \rho_{xx}(0T))/\rho_{xx}(0T) \times 100\%$. With decreasing temperature, the *MR* increases dramatically. At 1.5 K, the *MR* starts to oscillate at field as low as $B \approx$ 2 T, due to the high mobility of charge carriers. At 280 K, the *MR* is roughly linear, and there is no sign of saturation in high field, as high as 200% at 14.5 T. Such a linear quantum *MR* should result from the linear dispersion spectrum in both the valence and conduction bands, as proposed by Abrikosov[14]. Our observation of large linear *MR* at

280 K confirms the theoretical prediction[3], and supports the existence of 3D Dirac point

in Cd_3As_2.

In Fig. 2a, we show the oscillatory component of $\Delta\rho_{xx}$ versus $1/B$ at various

temperatures after subtracting a smooth background. They are periodic in $1/B$, as

expected from the successive emptying of Laudau levels E_n (LLs) when the magnetic

field is increased. A single oscillation frequency $F = 58.3$ T is identified from fast

Fourier transform (FFT) spectra, which corresponds to $\Delta(1/B) = 0.0171$ T^{-1}. According

to the Onsager relation $F = (\Phi_0/2\pi^2)A_k$, the cross-sectional area of the Fermi surface

normal to the field is $A_F = 5.6 \times 10^{-3}$ Å^{-2}. By assuming a circular cross section, the radius

$k_F = 0.042$ Å^{-1} is estimated.

The SdH oscillation amplitude can be described by the Lifshitz-Kosevich formula[22,23],

$$\Delta\rho_{xx} \propto \frac{\alpha T/\Delta E_n(B)}{\sinh\left[\alpha T/\Delta E_n(B)\right]} e^{-\alpha T_D/\Delta E_n(B)} \cos 2\pi \left(\frac{F}{B} + \gamma - \delta\right).$$

$\alpha = 2\pi^2 k_B$ and $\Delta E_n(B) = heB/2\pi m^*$ is the energy gap between the nth and $(n +$

1)th LL, where m^* is the effective mass of the carriers. T_D is the Dingle temperature.

$2\pi\gamma$ is the Berry's phase and δ is a phase shift governed by the curvature of the Fermi

surface, which will be discussed later. Figure 2b plots the temperature dependence of

the normalized oscillation amplitude at $1/B = 0.0928$ T^{-1}, which corresponds to the 6th

LL. The energy gap ΔE_n can be obtained from the thermal damping factor

$$R_T = \frac{\alpha T/\Delta E_n(B)}{\sinh\left[\alpha T/\Delta E_n(B)\right]}.$$

The solid line in Fig. 2b is the best fit to the data, which yields $\Delta E_{n=6}(B) = 24.6$ meV.

Similar processes can be done for the rest LLs. The obtained $1/\Delta E_n$ for different LLs

versus $1/B$ are plotted in Fig. 2c. The slope of the linear fitting gives a rather small

cyclotron mass $m^* = 0.037m_0$. The Fermi velocity then can be calculated as $\upsilon_F = \frac{\hbar k_F}{m^*} = 1.3 \times 10^6$ m/s, which is very close to the ARPES result 1.5×10^6 m/s (ref. 6).

Figure 3 is the Landau index plot, n versus $1/B$. According to the Lifshitz-Onsager quantization rule $A_F \frac{\hbar}{eB} = 2\pi(n + \gamma - \delta)$, the Landau index n is linearly dependent on $1/B$. Our data points in Fig. 3 fall into a very straight line, and the linear extrapolation gives an intercept 0.58(1). In the trivial parabolic dispersion case, the Berry's phase $2\pi\gamma$ should be zero, while $\gamma = 1/2$ corresponds to a nontrivial π Berry's phase expected for 2D Dirac fermions. It has been observed in graphene and the 2D surface state of topological insulators Bi_2Se_3 and Bi_2Te_3 (ref. 17, 19, 21). In quasi-2D and 3D Dirac materials, however, there should be a phase shift $|\delta| \leq 1/8$ on γ, resulting from the curvature of the Fermi surface in the third direction[20,22]. The intercept 0.58 we obtain for Cd_3As_2 means that there is an apparent phase shift $\delta = 0.08$ on the nontrivial π Berry's phase. Determining the phase factor γ and δ provides strong evidence for the existence of 3D Dirac fermions in Cd_3As_2..

To conclude, we have done bulk transport measurements on the proposed 3D Dirac semimetal Cd_3As_2 singel crystals. A sizable linear quantum magnetoresistance is observed near room temperature. Via analysis of the Shubnikov-de Haas oscillations of longitudinal resistivity in magnetic field, a nontrivial π Berry's phase with a phase shift is obtained. These bulk quantum transport results unambiguously confirm the 3D Dirac semimetal phase in Cd_3As_2, complementary to previous ARPES and STM experiments.

METHODS

The Cd_3As_2 single crystals were grown from Cd flux with starting composition Cd : As = 8 : 3, as described in ref. 24. The Cd and As powders were put in an alumina crucible after sufficient grinding. The alumina crucible was placed in an iron crucible, which was then sealed in argon atmosphere. The iron crucible was heated to 825 °C and kept for 24 hours, then slowly cooled down to 425 °C at 6 °C/hour. After the alumina crucible was taken out, the excess Cd flux was removed by centrifuging in a quartz tube at 425 °C. The largest natural surface of the obtained Cd_3As_2 single crystals was determined as (112) plane by X-ray diffraction, with typical dimension of 2.0×2.0 mm^2. The quality of Cd_3As_2 single crystals was further checked by X-ray rocking curve, shown in the inset of Fig. 1a. The sample was cut and polished to a bar-shape, with 1.70×0.78 mm^2 in the (112) plane and 0.20 mm in thickness. Standard six-probe method was used for both longitudinal resistivity and transverse Hall resistance measurements. Magnetic field was applied perpendicular to the (112) plane up to 14.5 T.

1. Young, S. M., Zaheer, S., Teo, J. C., Kane, C. L., Mele, E. J. & Rappe, A. M. Dirac semimetal in three dimensions. *Phys. Rev. Lett.* **108**, 140405 (2012).

2. Wang, Z. *et al*. Dirac semimetal and topological phase transitions in A_3Bi (A = Na, K, Rb). *Phys. Rev. B* **85**, 195320 (2012).

3. Wang, Z., Weng, H., Wu, Q., Dai, X. & Fang, Z. Three-dimensional Dirac semimetal and quantum transport in Cd_3As_2. *Phys. Rev. B* **88**, 125427 (2013).

4. Liu, Z. K. *et al*. Discovery of a three-Dimensional topological Dirac semimetal, Na_3Bi. *Science* **343**, 864-867 (2014).

5. Xu, S. -Y. *et al*. Observation of a bulk 3D Dirac multiplet, Lifshitz transition, and nestled spin states in Na_3Bi. arXiv:1312.7624

6. Neupane, M. *et al*. Observation of a topological 3D Dirac semimetal phase in high-mobility Cd_3As_2 and related materials. arXiv:1309.7892.

7. Borisenko, S., Gibson, Q., Evtushinsky, D., Zabolotnyy, V., Buechner, B. & Cava, R. J. Experimental realization of a three-dimensional Dirac semimetal. arXiv:1309.7978.

8. Jeon, S. *et al*. Landau quantization and quasiparticle interference in the three-dimensional Dirac semimetal Cd_3As_2. arXiv:1403.3446.

9. Castro Neto, A. H., Guinea, F., Peres, N. M. R., Novoselov, K. S. & Geim, A. K. The electronic properties of graphene. *Rev. Mod. Phys.* **81**, 109-162 (2009).

10. Hasan, M. Z. & Kane, C. L. Topological Insulators. *Rev. Mod. Phys.* **82**, 3045-3067 (2010).

11. Qi, X. -L. & Zhang, S. -C. Topological insulators and superconductors. *Rev. Mod. Phys.* **83**, 1057 (2011).

12. Xu, R., Husmann, A., Rosenbaum, T. F., Saboungi, M. L., Enderby, J. E. & Littlewood, P. B. Large magnetoresistance in non-magnetic silver chalcogenides. *Nature* **390**, 57-60 (1997).

13. Abrikosov, A. A. Quantum magnetoresistance. *Phys. Rev. B* **58**, 2788-2794 (1998).

14. Zhang, W., Yu, R., Feng, W., Yao, Y., Weng, H., Dai, X. & Fang, Z. Topological aspect and quantum magnetoresistance of β-Ag_2Te. *Phys. Rev. Lett.* **106**, 156808 (2011).

15. Tang, H., Liang, D., Qiu, R. L. & Gao, X. P. Two-dimensional transport-induced linear magneto-resistance in topological insulator Bi_2Se_3 nanoribbons. *ACS Nano* **5**, 7510-7516 (2011).

16. He, H. *et al.* High-field linear magnetoresistance in topological insulator Bi_2Se_3 thin films. *Appl. Phys. Lett.* **100**, 032105 (2012).

17. Qu, D. X., Hor, Y. S., Xiong, J., Cava, R. J. & Ong, N. P. Quantum oscillations and hall anomaly of surface states in the topological insulator Bi_2Te_3. *Science* **329**, 821-824 (2010).

18. Wang, X., Du, Y., Dou, S. & Zhang, C. Room temperature giant and linear magnetoresistance in topological insulator Bi_2Te_3 nanosheets. *Phys. Rev. Lett*. **108**, 266806 (2012).

19. Zhang, Y. B., Tan, Y. W., Stormer, H. L. & Kim, P. Experimental observation of the quantum Hall effect and Berry's phase in graphene. *Nature* **438**, 201-204 (2005).

20. Luk'yanchuk, I. A. & Kopelevich, Y. Dirac and normal fermions in graphite and graphene: implications of the quantum Hall effect. *Phys. Rev. Lett.* **97**, 256801 (2006).

21. Analytis, J. G., McDonald, R. D., Riggs, S. C., Chu, J. H., Boebinger, G. S. & Fisher, I. R. Two-dimensional surface state in the quantum limit of a topological insulator. *Nat. Phys.* **6**, 960-964 (2010).

22. Murakawa, H. *et al.* Detection of Berry's phase in a bulk Rashba semiconductor. *Science* **342**, 1490-1493 (2013).

23. Shoenberg, D. Magnetic oscillations in metals. *Cambridge Univ. Press*, (1984).

24. Ali, M. N., Gibson, Q., Jeon, S., Zhou, B. B., Yazdani, A. & Cava, R. J. The crystal and electronic structures of Cd_3As_2, the 3D electronic analogue to graphene. arXiv:1312.7576

Author Information The authors declare no competing financial interests. Correspondence and requests for materials should be addressed to S. Y. Li (shiyan_li@fudan.edu.cn).

Figure 1 | Longitudinal resistivity and Hall resistance of Cd_3As_2.

a. The longitudinal resistivity of Cd_3As_2 single crystal in zero magnetic field, with current in the (112) plane. The X-ray rocking curve of (224) peak is shown in the inset. The full-width at half-maximum (FWHM) is only 0.08°, indicating the high quality of the single crystals. **b.** The Hall resistance R_{xy} from 200 K down to 1.5 K. The oscillations of R_{xy} are visible blow 50 K. **c.** The Shubinikov-de Haas oscillations of magnetoresistance from 280 K down to 1.5 K, with field perpendicular to the (112) plane. The magnetoresistance is defined by $MR = (\rho_{xx}(B) - \rho_{xx}(0T))/\rho_{xx}(0T) \times 100\%$. At 280 K, the MR is roughly linear without saturation, as high as 200% at $B = 14.5$ T. At 1.5 K, the oscillations appear at field as low as 2 T, indicating the high mobility of charge carriers in Cd_3As_2.

Figure 2 | Oscillatory component of longitudinal resistivity.

a. The oscillatory component $\Delta\rho_{xx}$, extracted from $\rho_{xx}(B)$ by subtracting a smooth background, as a function of $1/B$ at various temperatures. A single oscillation frequency $F = 58.3$ T is identified from fast Fourier transform (FFT) spectra. **b.** The temperature dependence of the relative amplitude of SdH oscillation in $\Delta\rho_{xx}(B)$ for the 6th Landau level. The solid line is a fit to the Lifshitz-Kosevich formula, from which we can extract the energy gap ΔE_n of the 6th Landau level. **c.** $1/\Delta E_n$ as a function of $1/B$, which is the position of the minimum in $\Delta\rho_{xx}$ for each Landau level. The slope of the linear fit gives the effective mass $m^* = 0.037m_0$.

Figure 3 | Nontrivial π Berry's phase in Cd_3As_2.

Landau index n plotted against $1/B$. The closed circles denote the integer index (ρ_{xx} valley), and the open circles indicate the half integer index (ρ_{xx} peak). This index plot is quite linear, giving an intercept 0.58 ± 0.01. From the inset, the intercept lies between γ and $\gamma + 1/8$ ($\gamma = 1/2$), which is a strong evidence for nontrivial π Berry's phase of 3D Dirac electrons in Cd_3As_2.

Figure 1

Figure 2
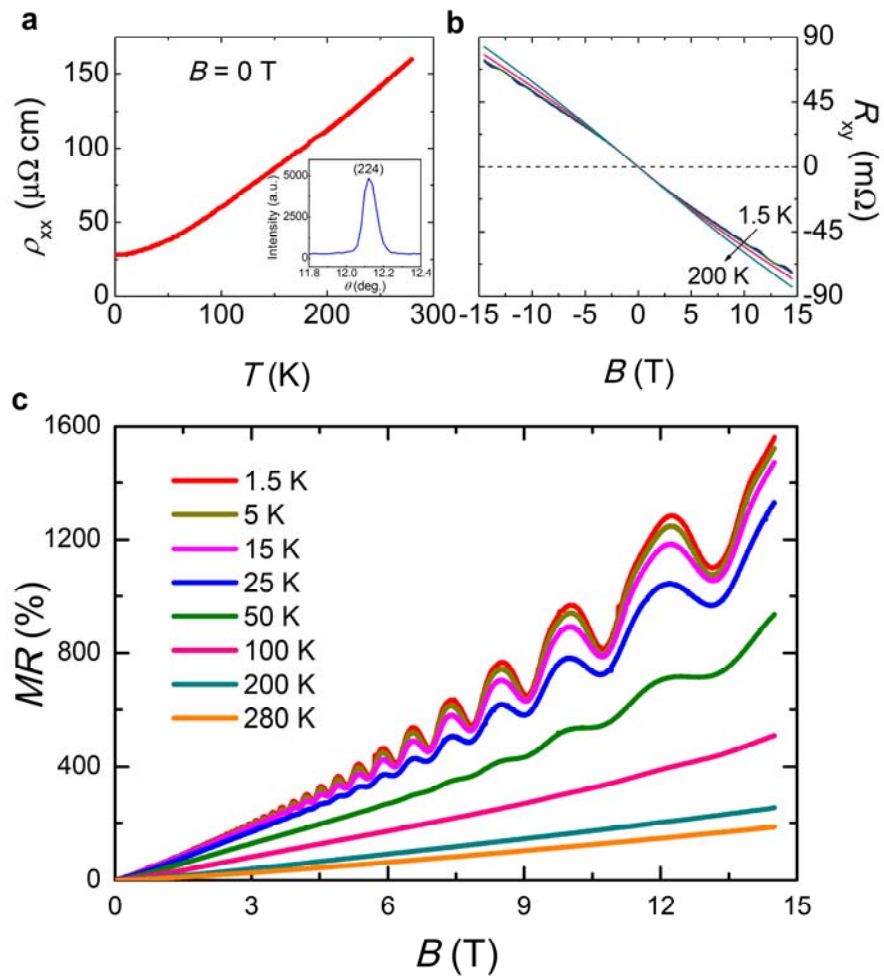
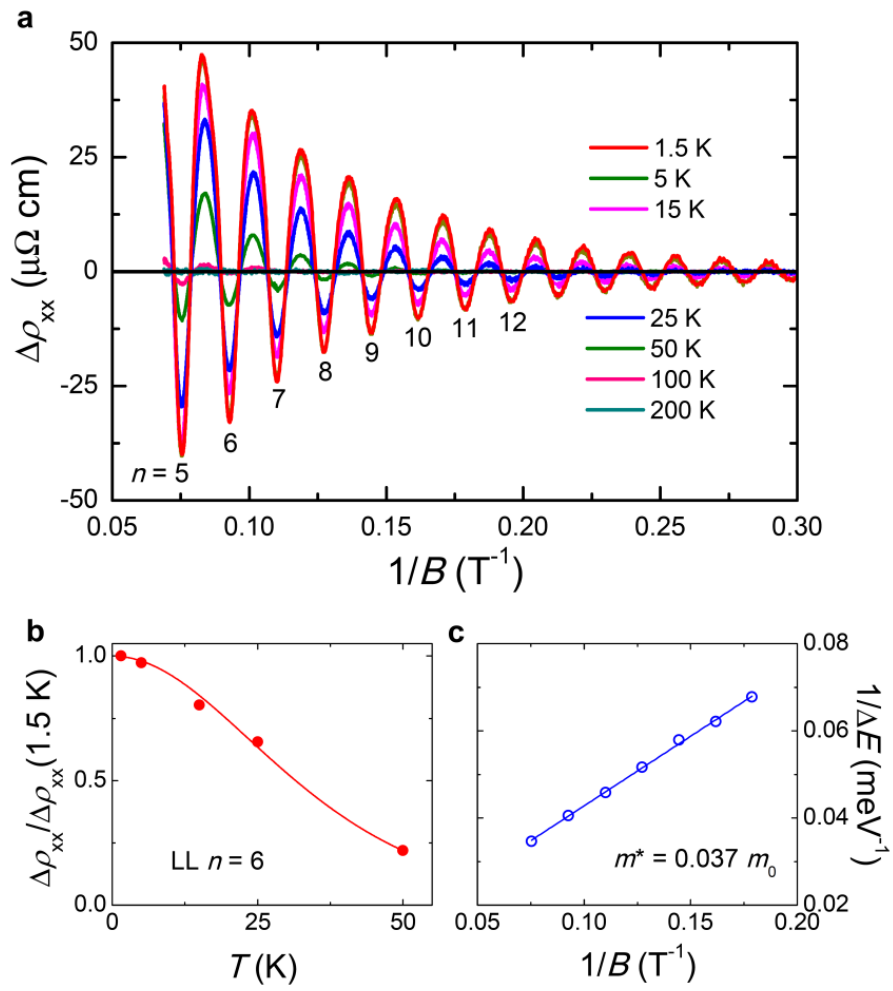**Figure 3**